Chapter 11: Regional Climate Projections

Coordinating Lead Authors: Jens Hesselbjerg Christensen and Bruce Hewitson

Lead Authors: Aristita Busuioc, Anthony Chen, Xuejie Gao, Isaac Held, Richard Jones, Won-Tae Kwon, René Laprise, Victor Magaña, Linda Mearns, Claudio Menendez, Jouni Räisänen, Annette Rinke, Rupa Kumar Kolli, Abdoulaye Sarr, Penny Whetton

Contributing Authors: Rasmus Benestad, Martin Beniston, David Bromwich, Josefino Comiso, Ramón de Elía, Klaus Dethloff, Seita Emori, Johannes Feddema, Ruediger Gerdes, Fidel Gonzales-Rouco, William J. Gutowski, Ingre Hansen-Bauer, Colin Jones, Robert Katz, Akio Kitoh, Reto Knutti, Ruby Leung, Jason Lowe, Amanda Lynch, Christoph Matulla, Kathleen McInnes, Brett Mullan, Mark New, David Plummer, Markku Rummukainen, Christoph Schär, Samuel Somot, Ramasamy Suppiah, Mark Tadross, Claudia Tebaldi, Warrant Tennant, Martin Widman, Rob Wilby

Review Editors: Congbin Fu, Filippo Giorgi

Date of Draft: 13 August 2005

Notes: This is the TSU compiled version

Figures

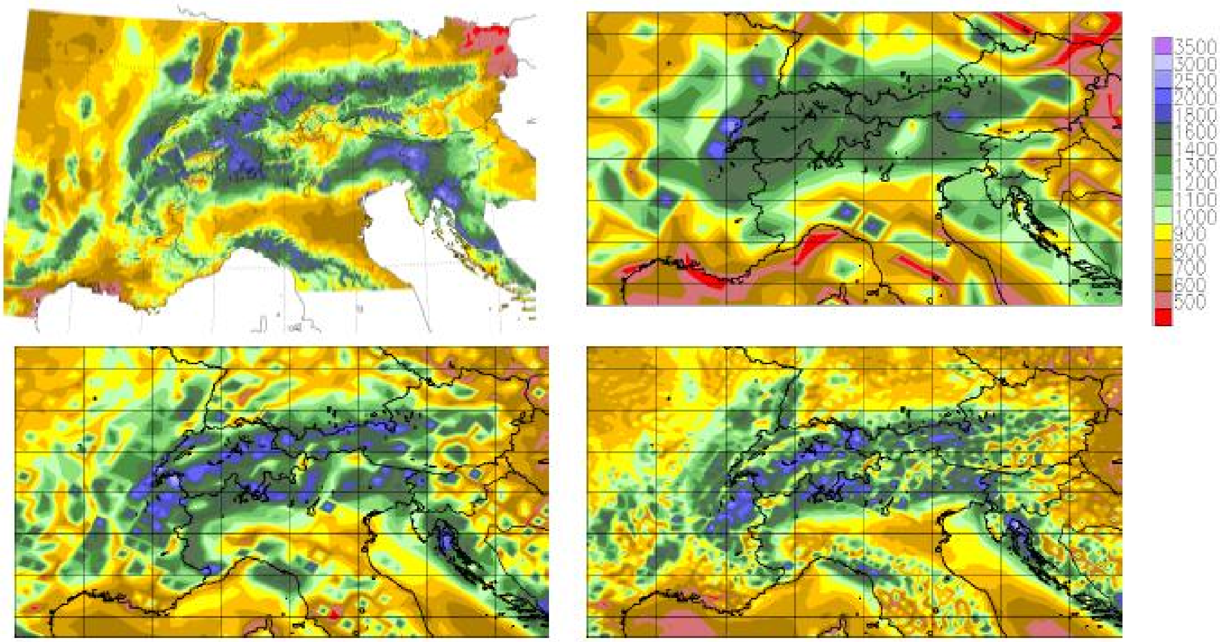

Figure 11.1.1. Annual mean precipitation for the European Alps (in mm). Upper left: Observational analysis (from Schwarb et al., 2001). Other panels RCM simulation at 50 km, 25 km, and 12 km inter grid distance. (From Christensen & Christensen, 2005).

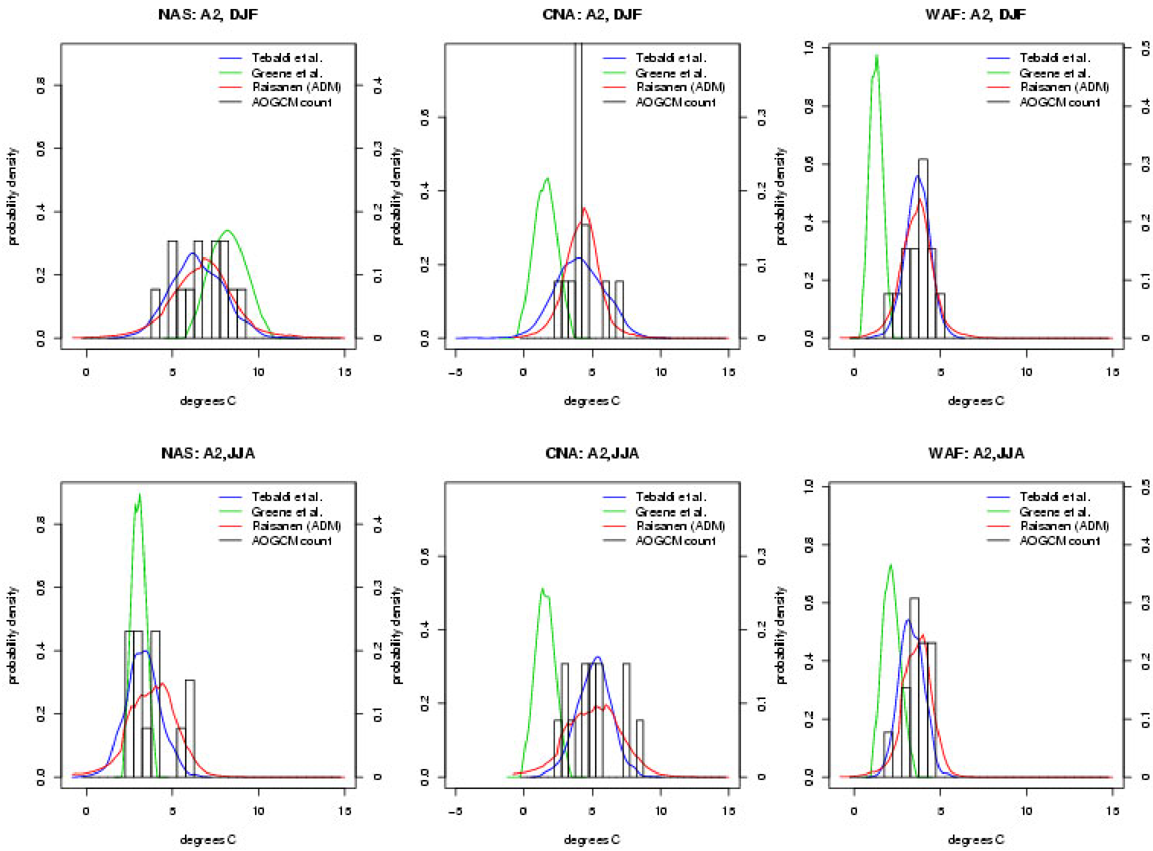

Figure 11.2.1. Comparison of Regional Probability Distribution Functions derived by three alternative methods. Each panel represents temperature change projections for the A2 SRES scenario for a combination of regions (Northern Asia (NAS),central North America (CAN) and western equatorial Africa (WAF)) and season (DJF and JJA). In each panel the three curves show alternative PDFs estimations, based on Tebaldi et al. (2005) (with natural variability accounted for), Greene et al. (2005), and Raisanen (2005). The histogram is derived by counting the fraction of AOGCMs whose projections fall in each of 30 bins, spanning the range of the x-axis by a 0.5 degree resolution. The scale on the left axis is the probability density scale. With respect to it, the integral under the curves (and the sum of the histogram bars' areas) is one. The scale to the right can be used to read the relative frequency from the histogram. The height of each bar indicates on this scale the fraction of models' projections out of the total falling in the corresponding interval.

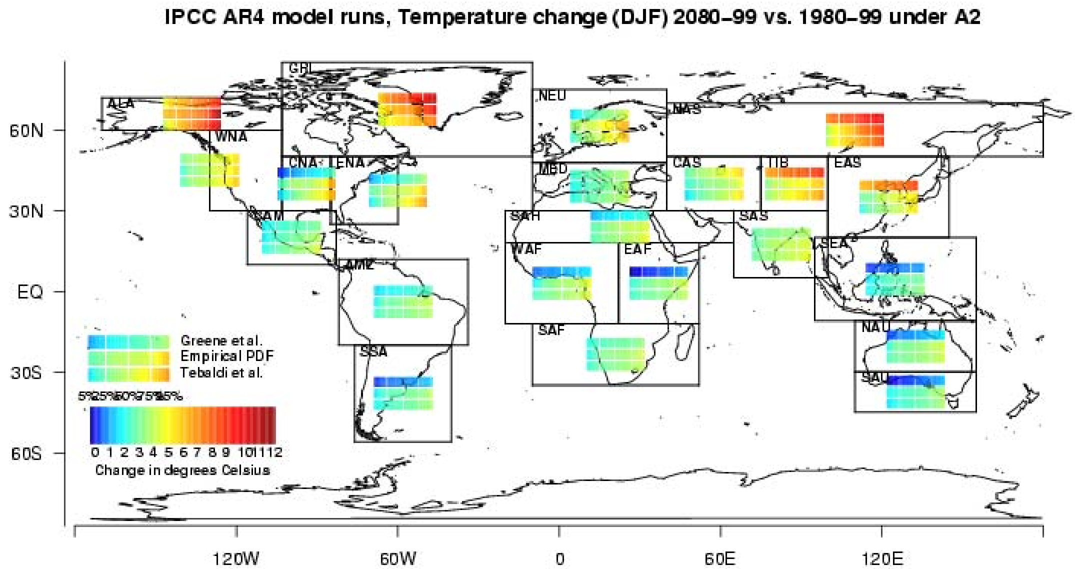

Figure 11.2.2. Quantiles of regional probability distributions derived by Greene et al. (top bar), Tebaldi et al. (bottom), and the empirical distribution of the AOGCM responses (middle bar) for temperature change in DJF under the A2 emissions scenario, at the end of the 21st century. Color bars indicate the 5–95% confidence interval. Lines through bars indicate the 25th, 50th, 75th, quantiles.

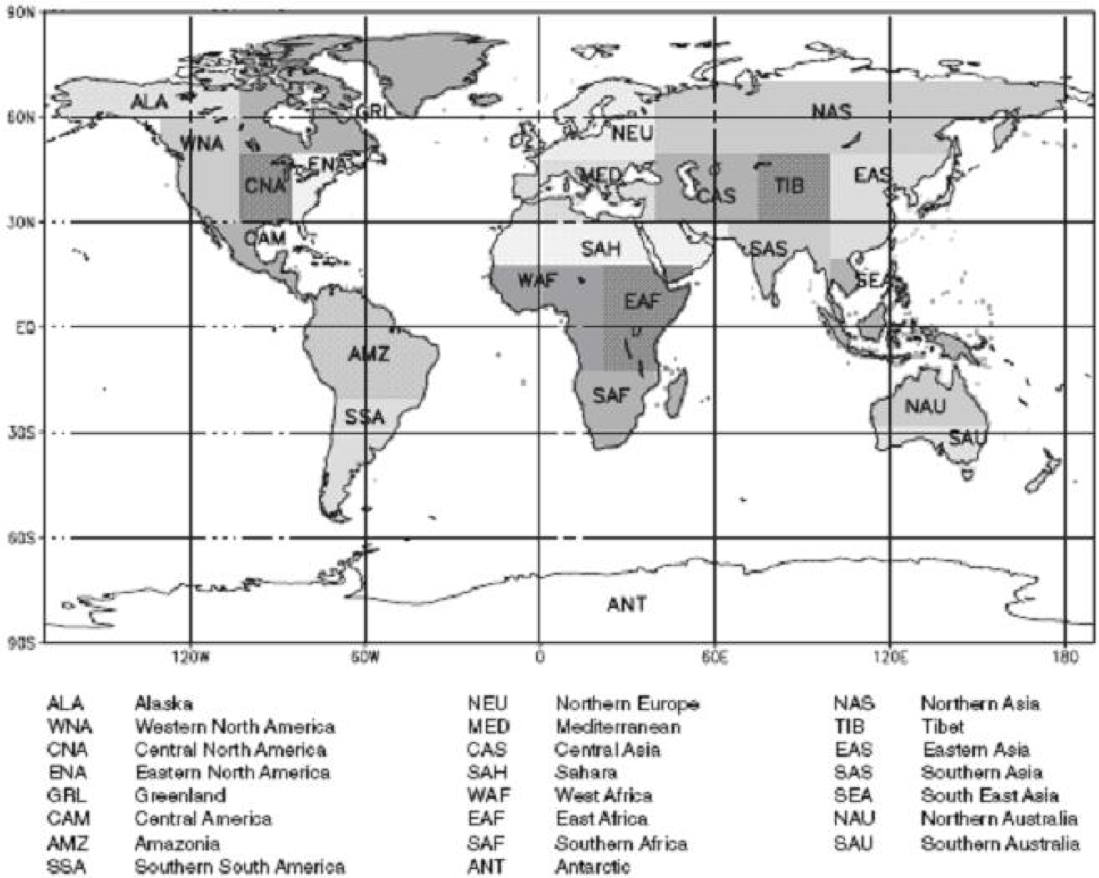

Figure 11.3.1.1. Regions used for the analysis presented in the regional sub-sections (from Giorgi and Francisco, 2000). [to be updated]

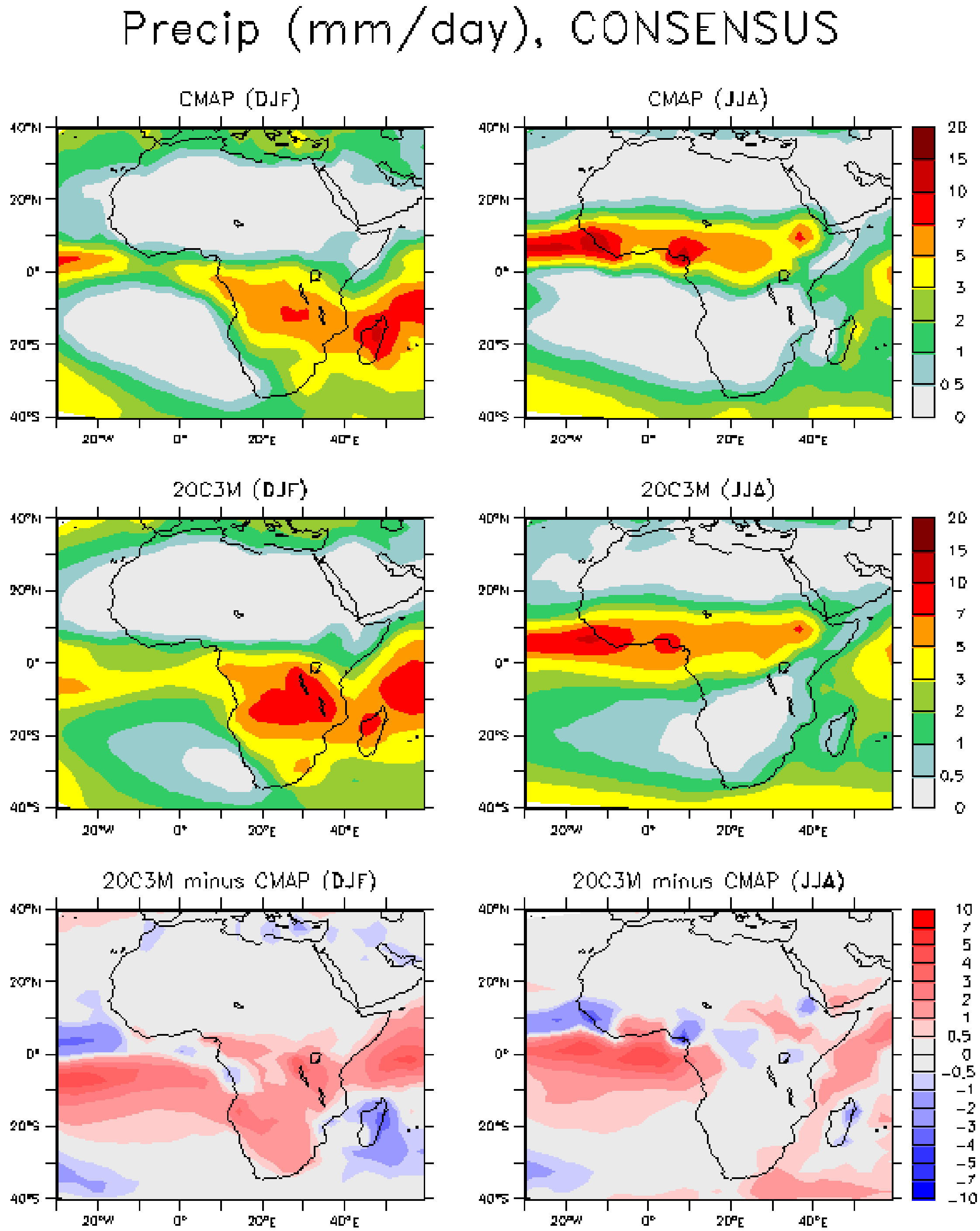

Figure 11.3.2.1. Mean daily precipitation (mm) for December-February (DJF) and June-August (JJA). Top panel is observed precipitation from CMAP. Middle panel id the multi-model mean for the 20th century simulation averaged over the period 1979–1999. The lower panel is the anomaly between the multi-model mean and CMAP.

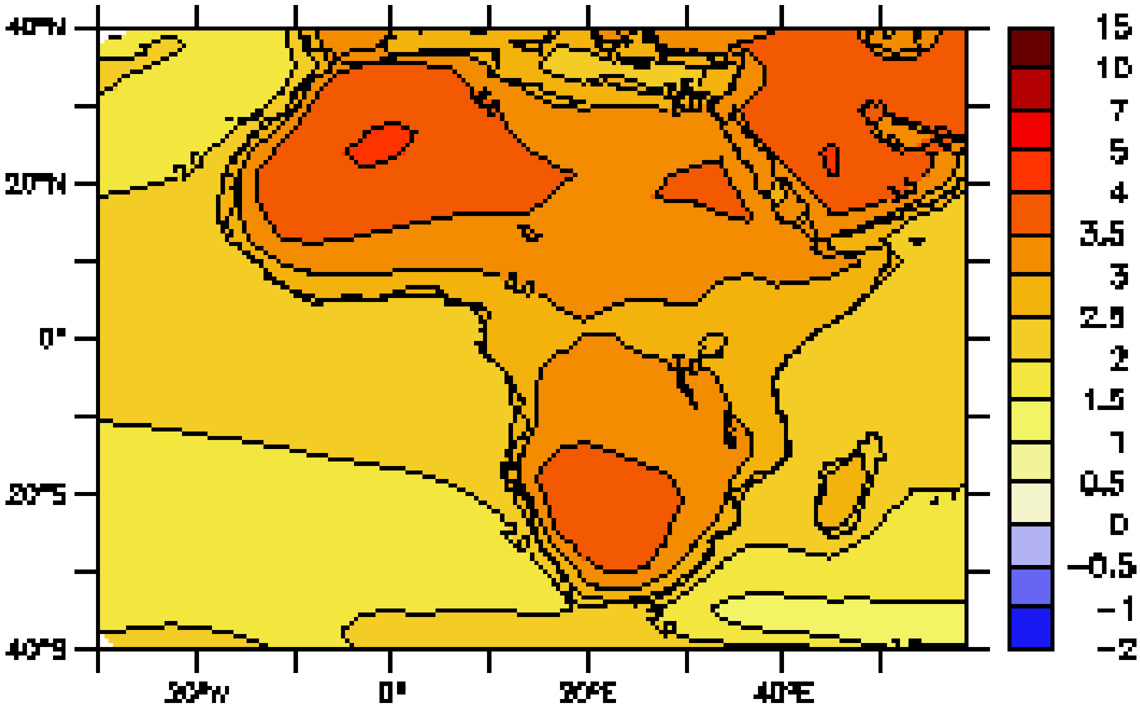

Figure 11.3.2.2. The annual mean temperature response over Africa averaged over all models in the PCMDI/AR4 archive for the A1B scenario (difference between 2079–2099 of SRESA1B and 1979–1999 of 20C3M)

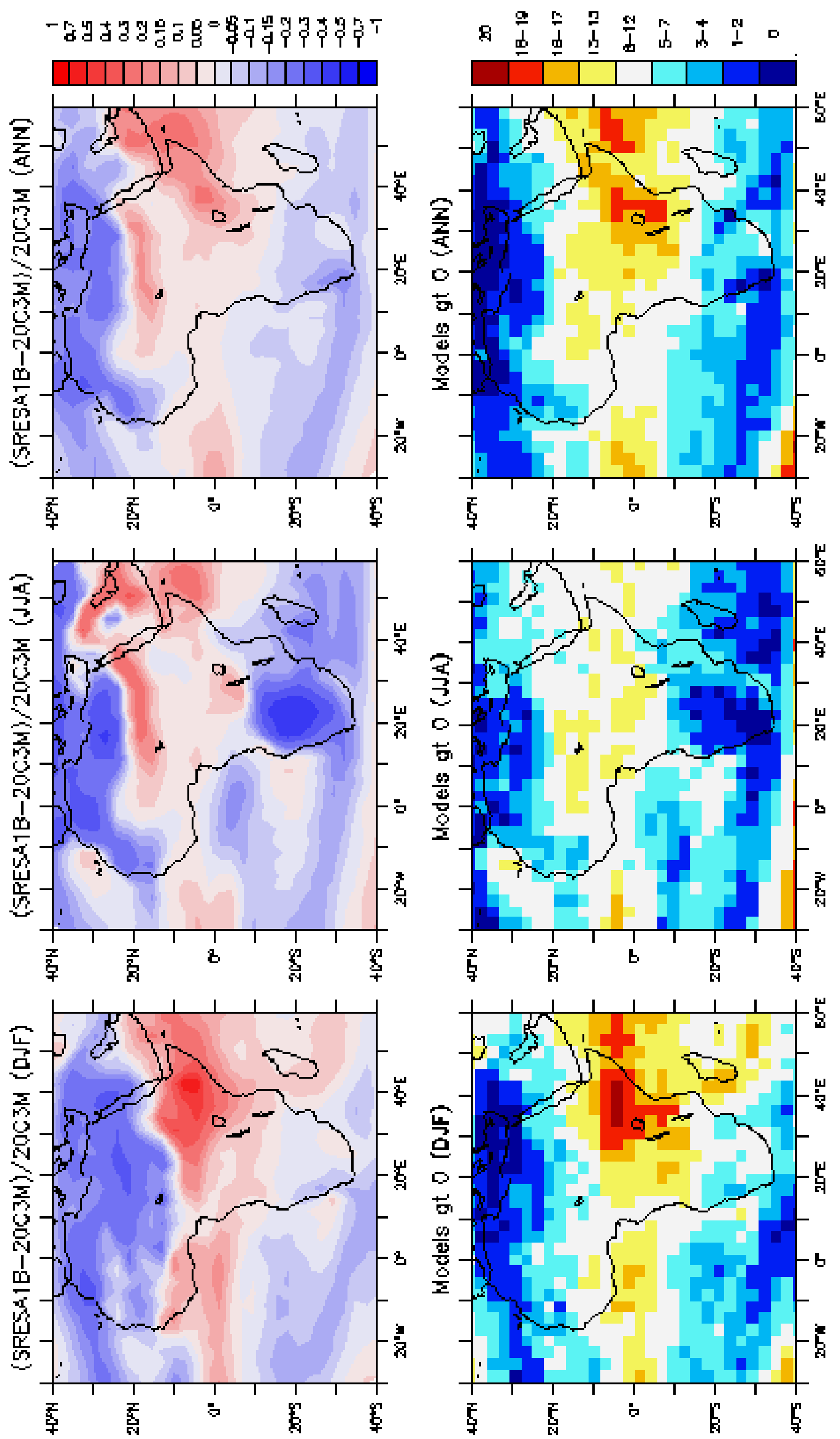

Figure 11.3.2.3. Robustness of climate change precipitation response from models in the AR4/PCMDI archive. Top panel shows the December-February (DJF), June-August (JJA) and annual (ANN) precipitation anomaly between 2079–2099 and 1979–1999 periods. The lower panel shows the number of models (out of 20) that predict mositening at a given location.

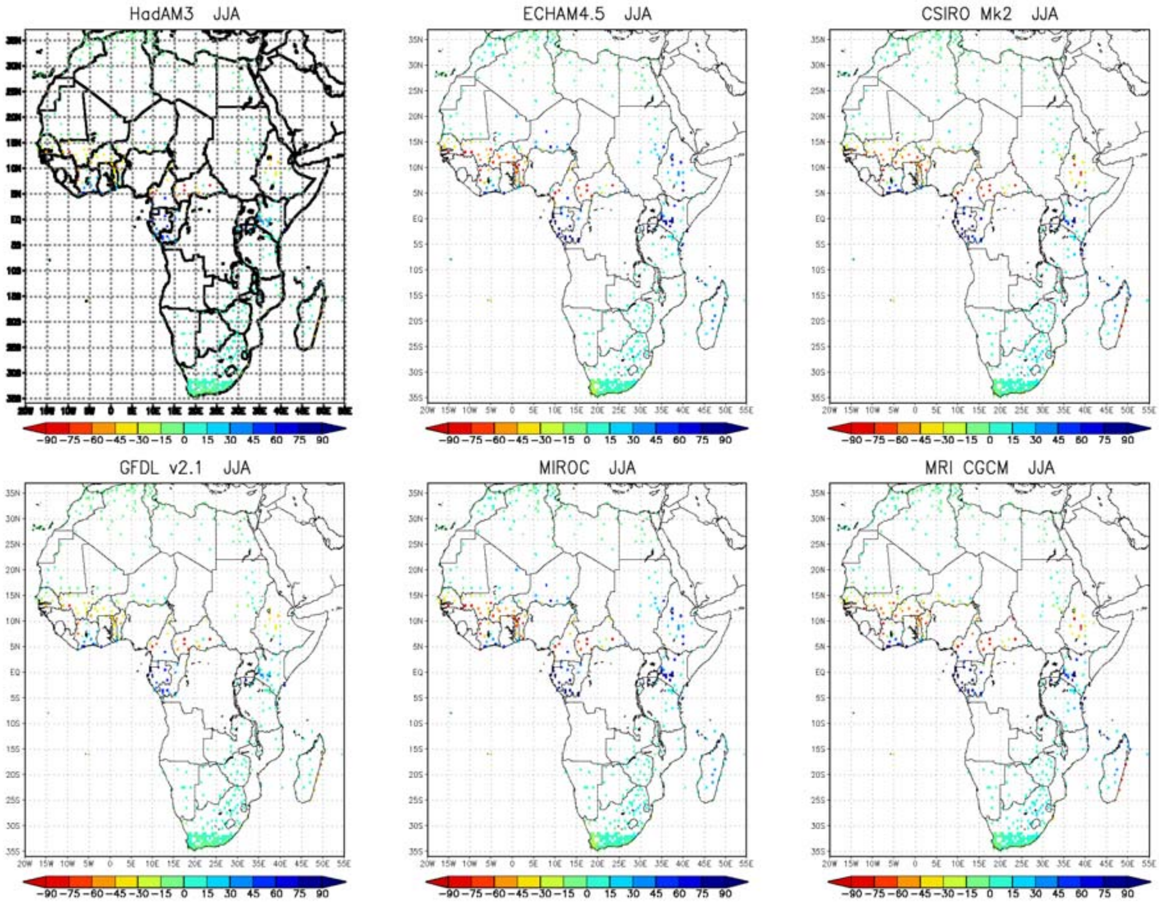

Figure 11.3.2.4. Anomaly of mean monthly precipitation (mm) daily data empirically downscaled from 6 GCMs (ECHAM4.5, HadAM3, CSIRO Mk2, GFDL 2.1, MRI, MIROC). GCMs are forced by the SRES A2 scenario. Anomalies are for the future period (2070–2099 for the first three models, and 2080–2099 for the latter three models) minus a control 30 year period.

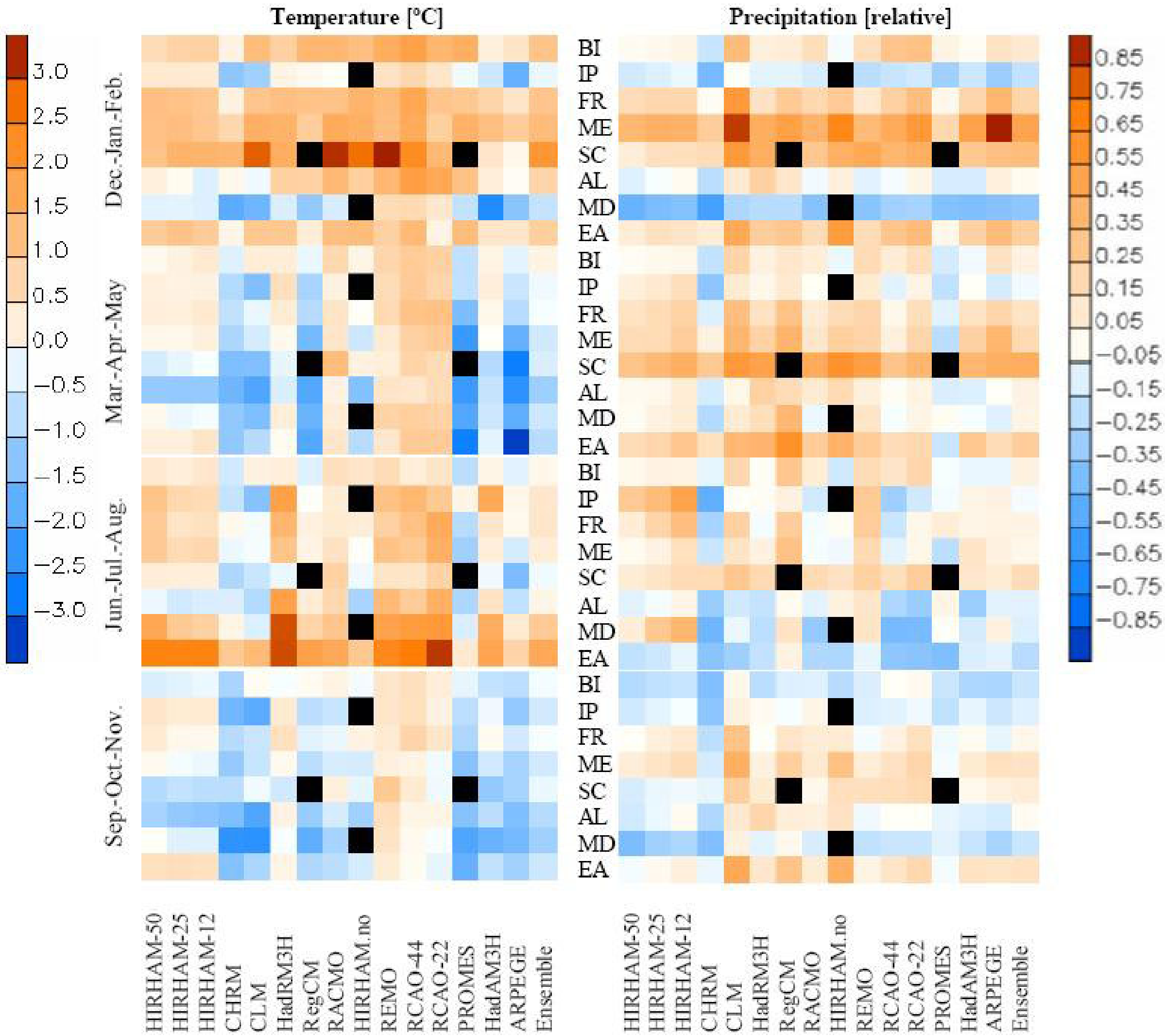

Figure 11.3.3.1. A schematic overview of seasonal biases of the PRUDENCE regional models. In each panel, rows are the analysis areas, columns correspond to models. Rows of panels signify the four seasons, the left column of panels are temperature biases (left color bar, degrees C), whereas the right column of panels signifies precipitation (right color bar, relative change). The label HIRHAM.no indicates the simulations done at met.no, as opposed to the HIRHAM simulations done at the DMI. Areas not covered by a particular model are indicated by black squares. 1=BI, 2=IP, 3=FR, 4=ME, 5=SC, 6=AL, 7=MD, 8=EA in Box 11.2, Figure 1 (Jacob et al., 2005).

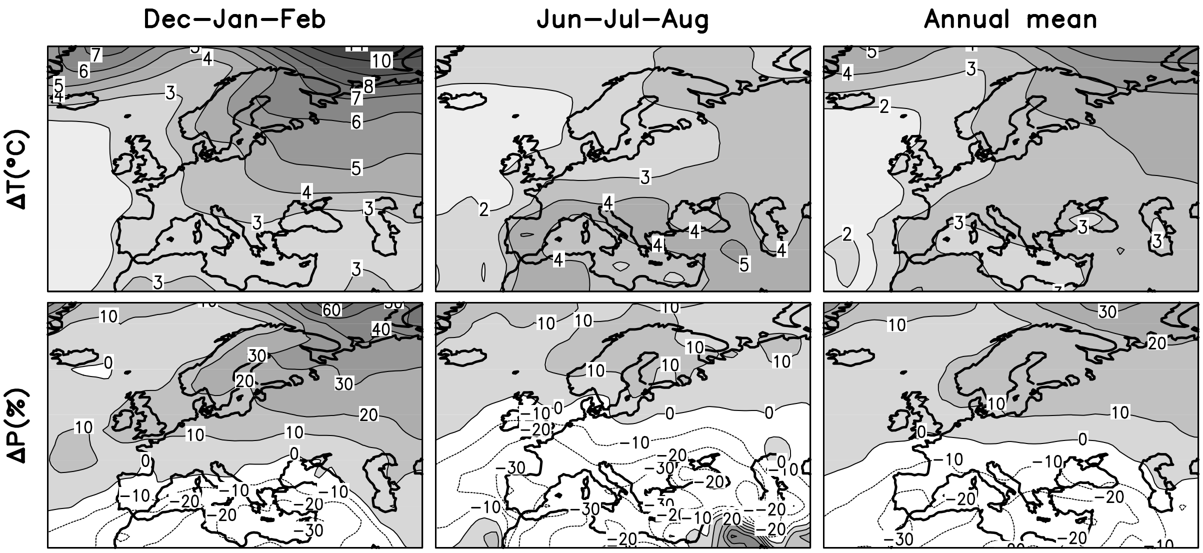

Figure 11.3.3.2. Multi-model mean changes in temperature (°C) and precipitation (%) from 1979–1998 to 2079–2098 under the SRES A1B emissions scenario.

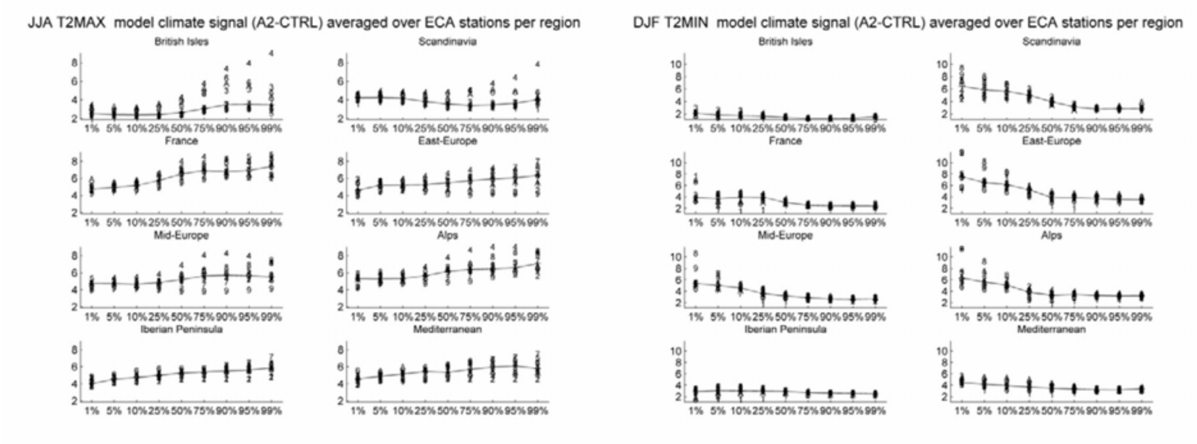

Figure 11.3.3.3. Changes in the distribution of JJA daily maximum temperatures and DJF daily minimum temperatures in various parts of Europe in HadAM3H-driven PRUDENCE simulations (from 1961–1990 to 2071–2100 under the SRES A2 emissions scenario). The horizontal axis gives the percentile of the distribution; for example, 95% of the daily minimum or maximum temperatures are lower than the 95th percentile. The vertical axis gives the changes in each percentile (in °C) separately for eight RCMs (1–8). The lines show the median of the eight RCM projections (Kjellström et al., 2005).

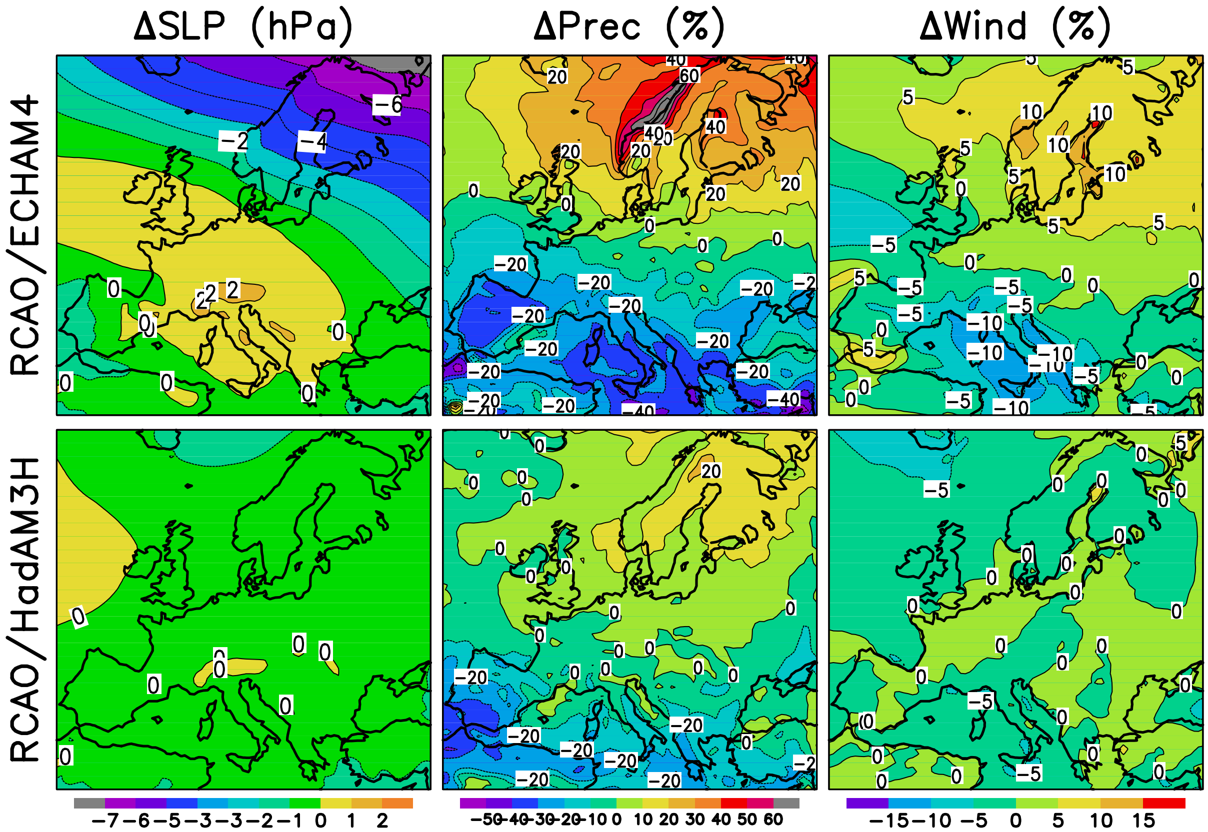

Figure 11.3.3.4. Simulated changes in annual mean sea level pressure (ΔSLP), precipitation (ΔPrec) and mean 10 m level wind speed (ΔWind) from the years 1961–1990 to the years 2071–2100. The results are based on the SRES A2 forcing scenario and were produced by the Rossby Centre RCM (RCAO) using boundary data from two global models: ECHAM4/OPYC3 (top) and HadAM3H (bottom) (redrawn from Rummukainen et al., 2004).

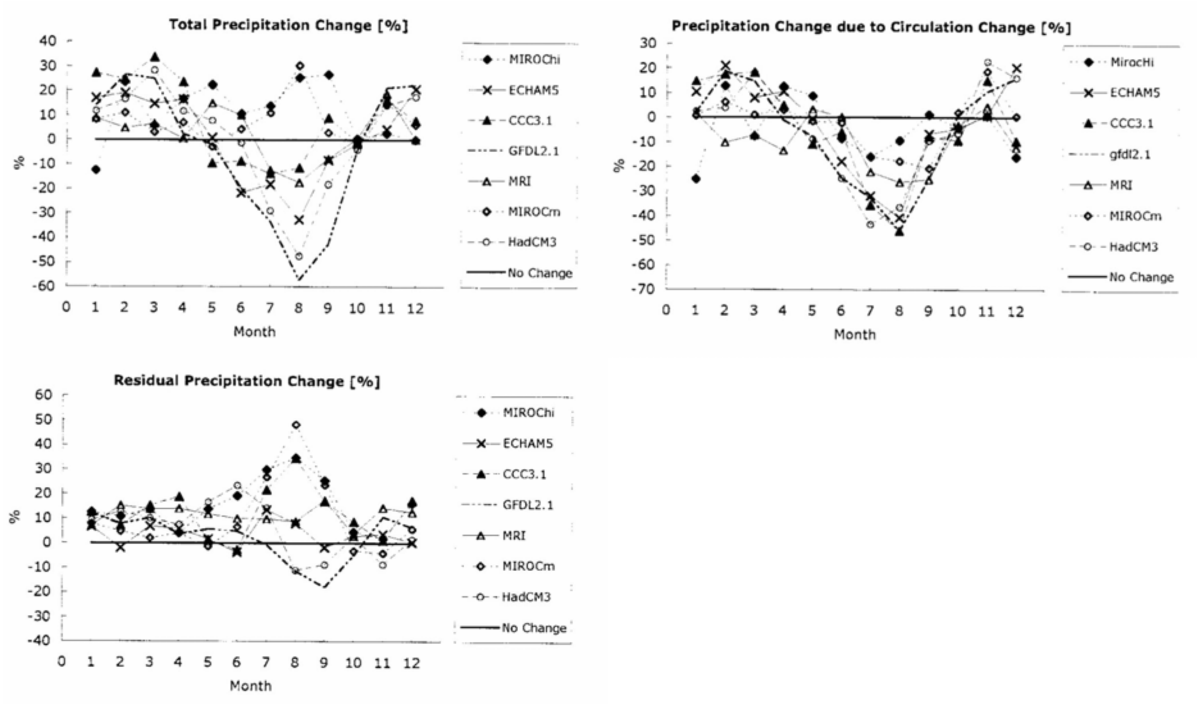

Figure 11.3.3.5. Changes in precipitation in western-central Europe (6–14°E, 48.5–53.5°N) from the 20th century to 2071–2100 (SRES A2 scenario) in seven AOGCMs. (a) total change, (b) estimated contribution of circulation change, (c) residual change [=(a)-(b)] (van Ulden and van Oldenborgh, 2005).

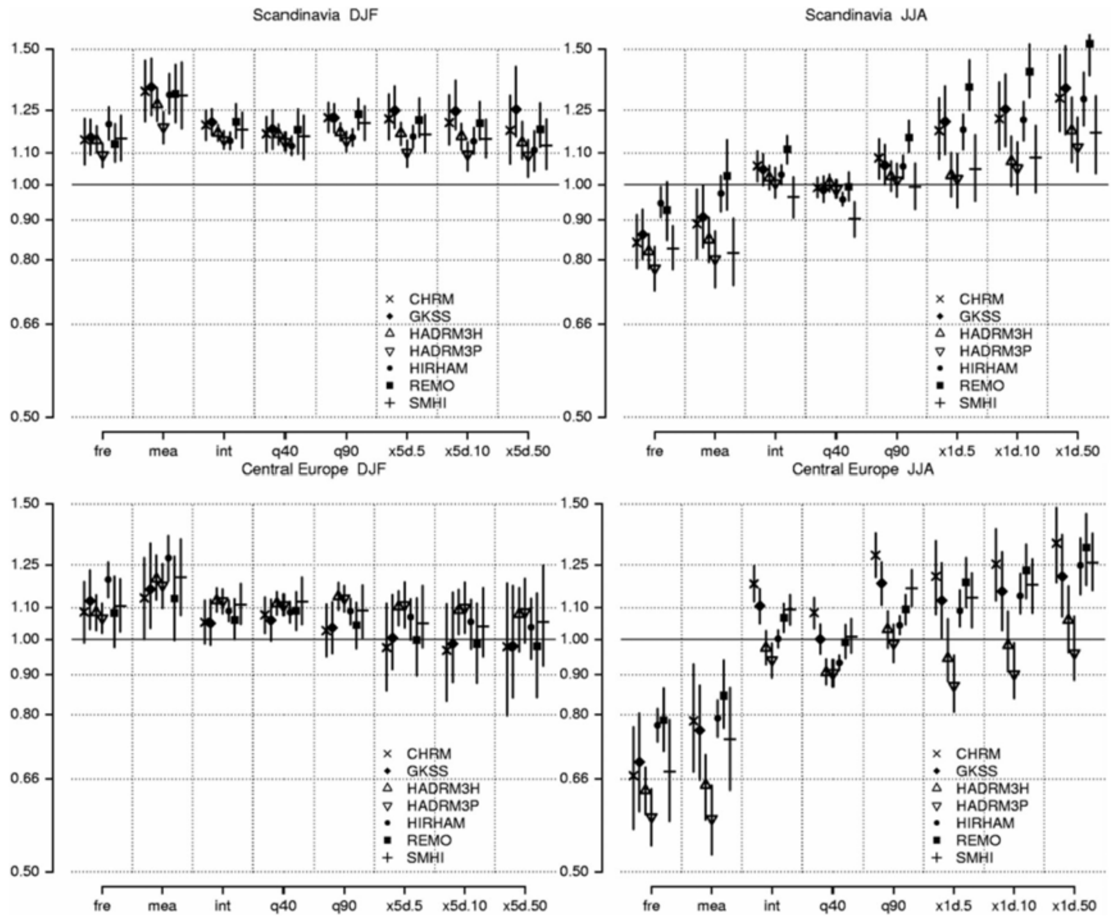

Figure 11.3.3.6. Changes (ratio 2071–2100/1961–1990) in domain-averaged precipitation statistics in the PRUDENCE simulations in southern Scandinavia (5–20°E, 55–62°N) and central Europe (5–15°E, 48–54°N) in winter (left) and in summer (right). *fre* = frequency of wet days; *mea* = total precipitation; *int* = mean precipitation for wet days; *q40* and *q90* = 40th and 90th percentiles of wet-day precipitation; *x1d.5 – x1d.50* = 5-to-50-year return values of one-day precipitation; *x5d.5 – x5d.50* = 5-to-50-year return values of five-day precipitation. Results are shown for seven RCMs. For each model, the vertical bar gives the 95% confidence range associated with sampling uncertainty. The figure indicates an unproportional increase in extreme precipitation in winter but not in summer (Frei et al., 2005).

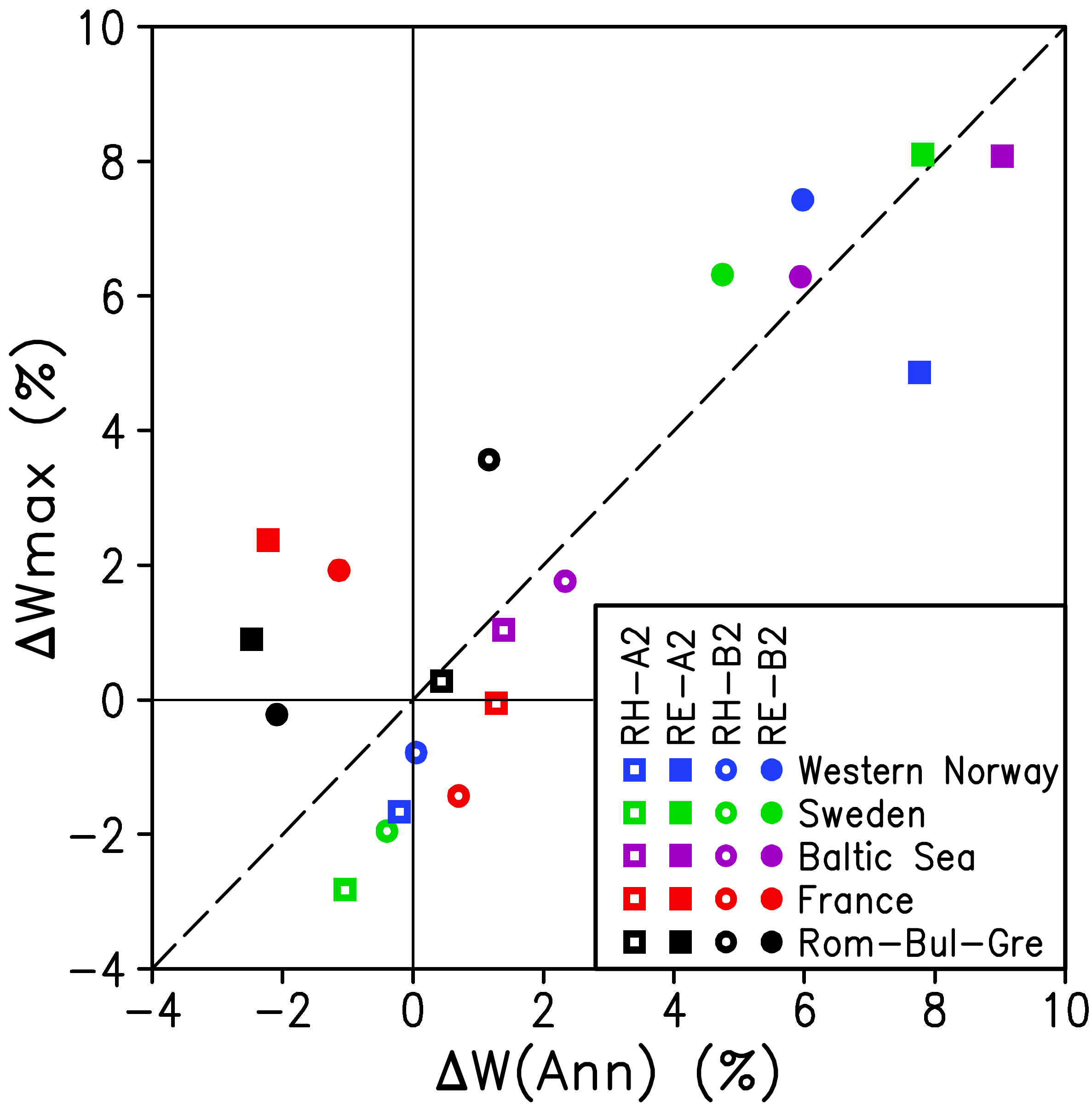

Figure 11.3.3.7. Changes in annual mean wind speed and average yearly maximum wind speed from the period 1961–1990 to the period 2071–2100, as evaluated from simulations made with the Rossby Centre RCM (Räisänen et al., 2004). As specified by the legend, results are shown for five European regions and four simulations using two different driving models and two emissions scenarios (RH-A2 – HadAM3H / SRES A2; RE-A2 – ECHAM4/OPYC3 / SRES A2; RH-A2 – HadAM3H / SRES B2; RE-B2 – ECHAM4/OPYC3 / SRES B2).

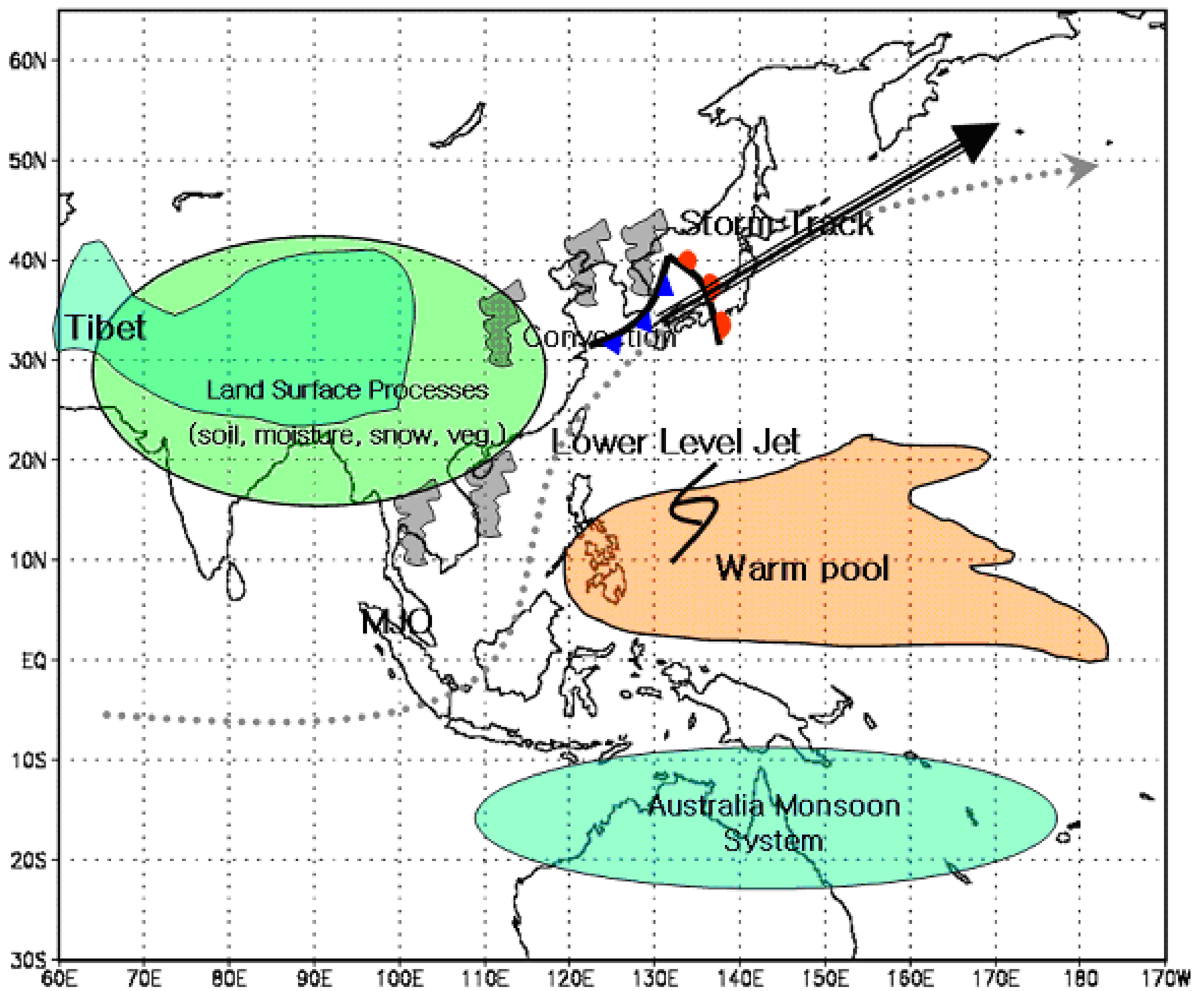

Figure 11.3.4.1. Summary of key processes in East Asia (modified from Kang et al., 2004)

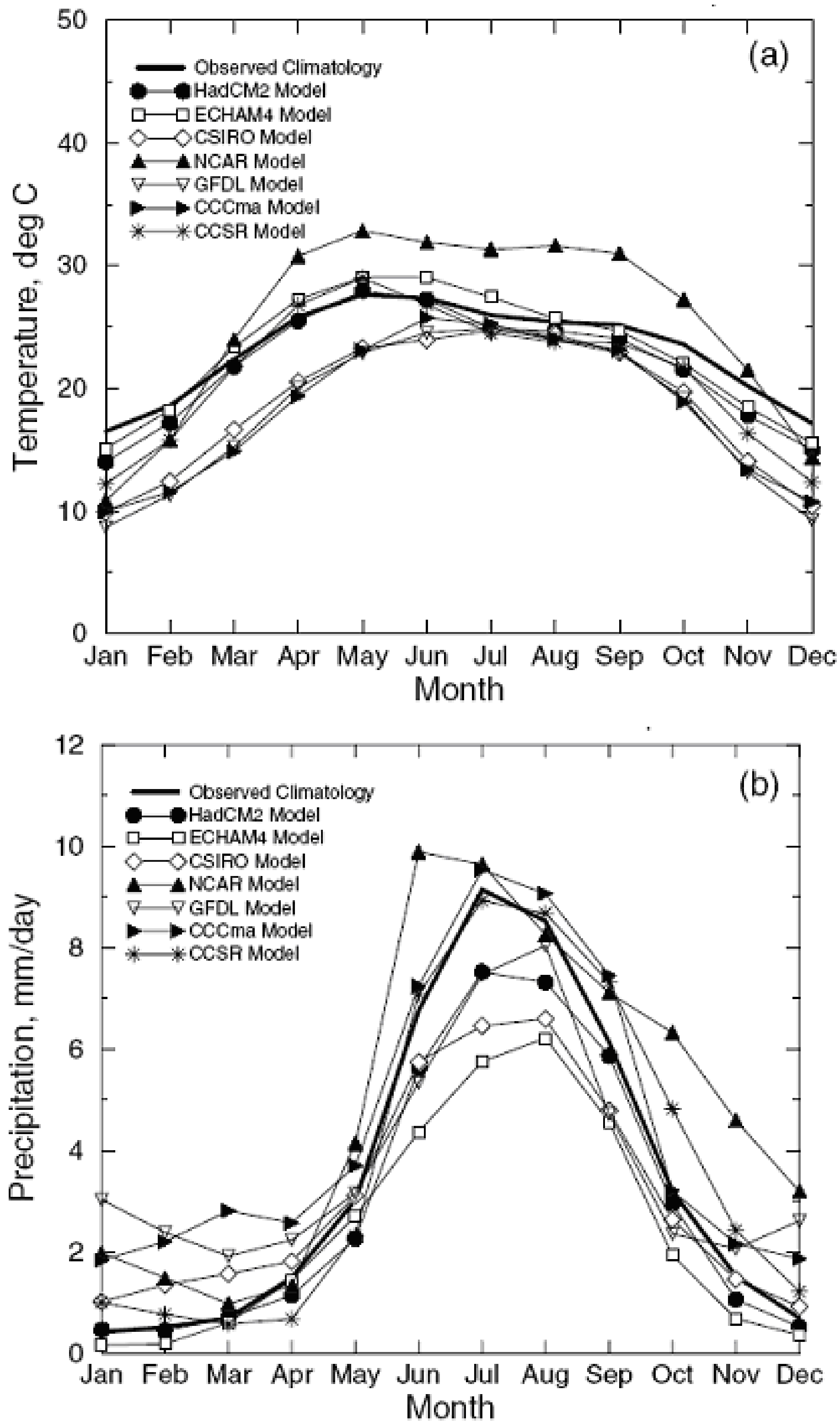

Figure 11.3.4.2. Validation of simulated and observed area-averaged annual cycle of (a) surface air temperature and (b) precipitation over South Asia. (After Lal and Harasawa, 2000).

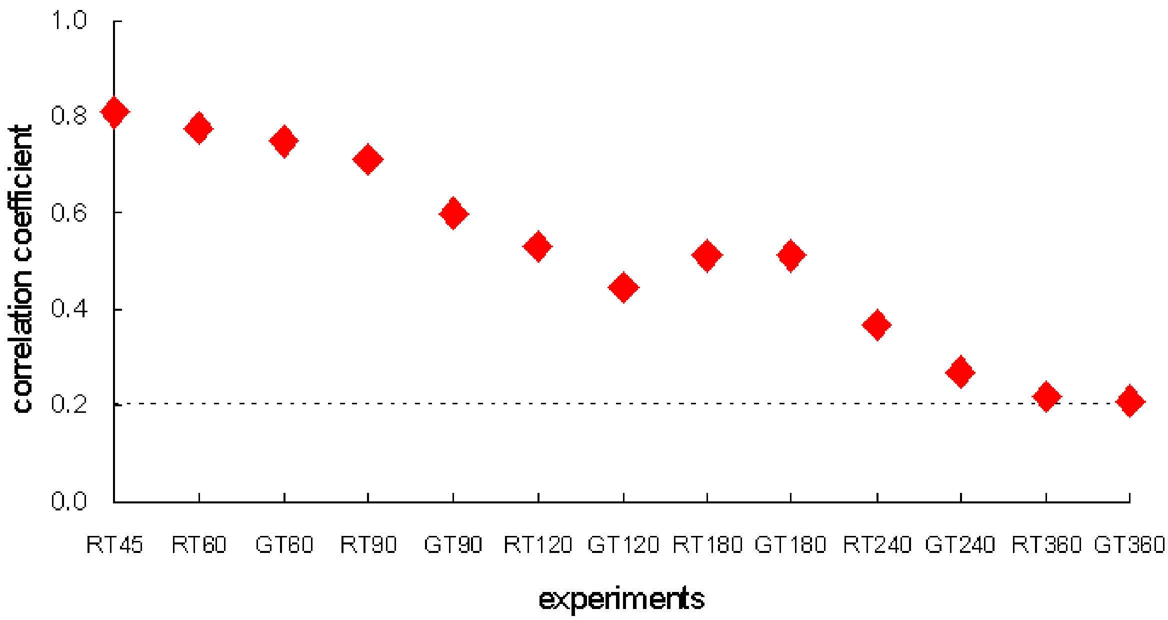

Figure 11.3.4.3. Spatial correlation coefficient between simulated and observed annual mean precipitation (RT45, RT60 … in the figure refered to the 45 km and 60 km … resolution with RegCM topography while GT60, GT90 refered to 60 km, 90 km … resolution with CSIRO topography. Dashed line is 0.99 significant level) (Gao et al., 2005)

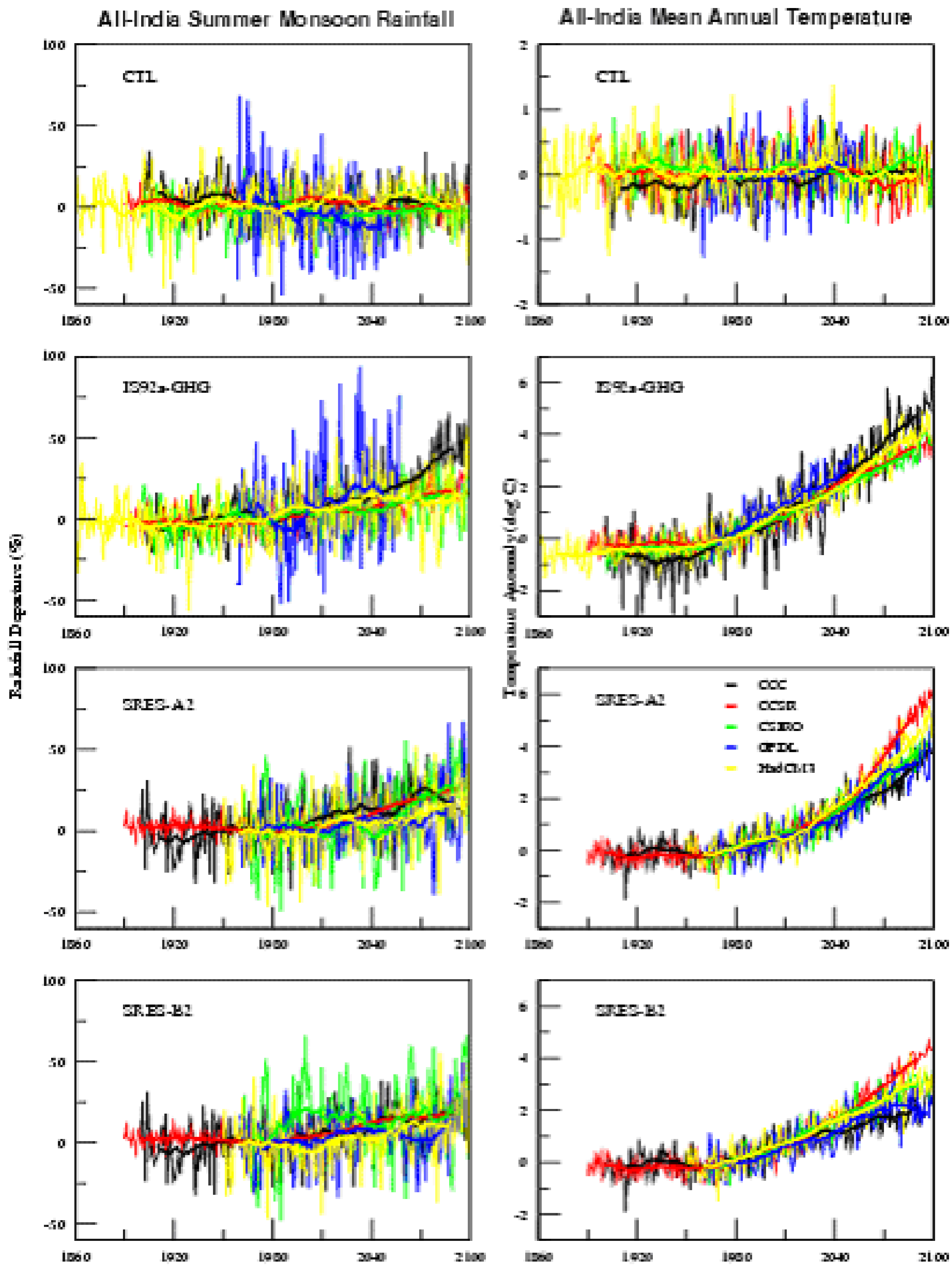

Figure 11.3.4.4. AOGCM projections of all-India mean summer monsoon rainfall and mean annual surface air temperature up to the year 2100, for IS92a and SRES A2 and B2 scenarios (After Rupa Kumar et al., 2003).

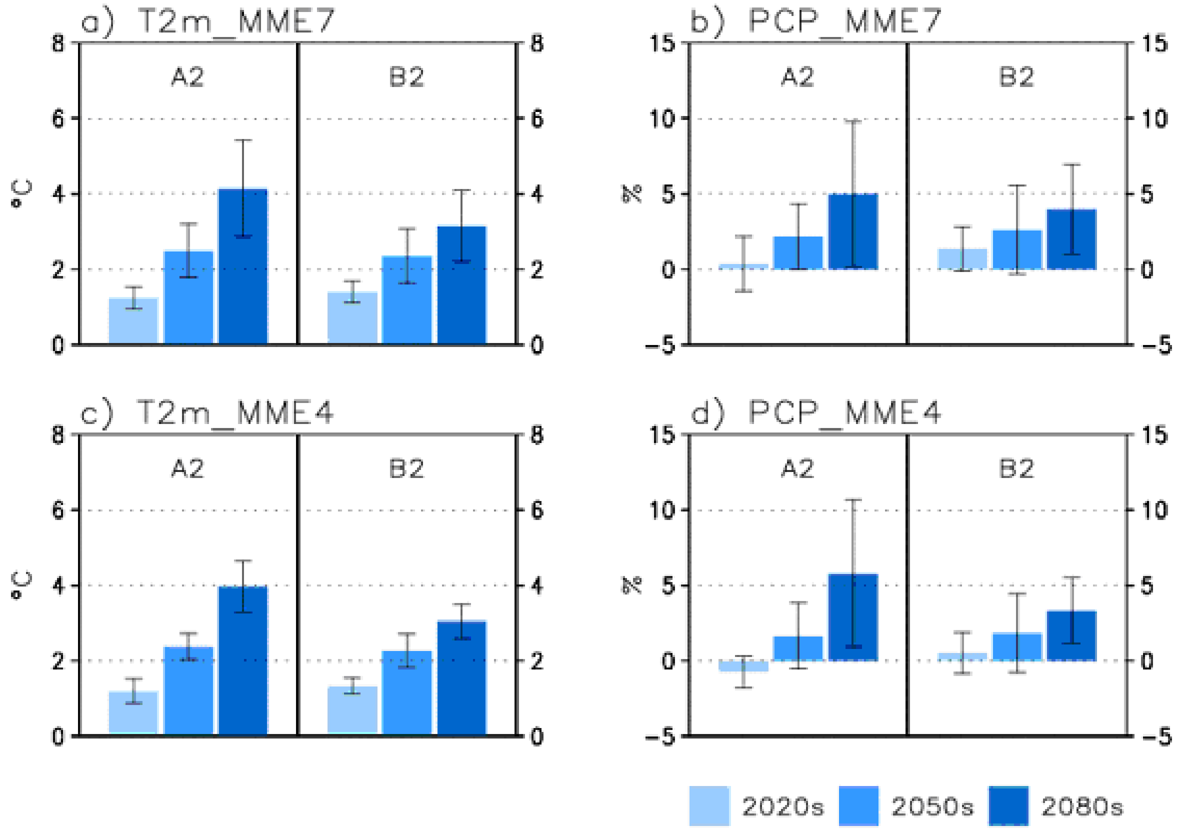

Figure 11.3.4.5. East Asian area-averaged temperature (°C) and precipitation changes (%) (bar) during 2020s, 2050s, and 2080s and their inter-model variability (error bar) from MME7 and MME4 for the SRES A2 and B2 scenarios. Changes are relative to 1961–1990 mean. (Min et al., 2004)

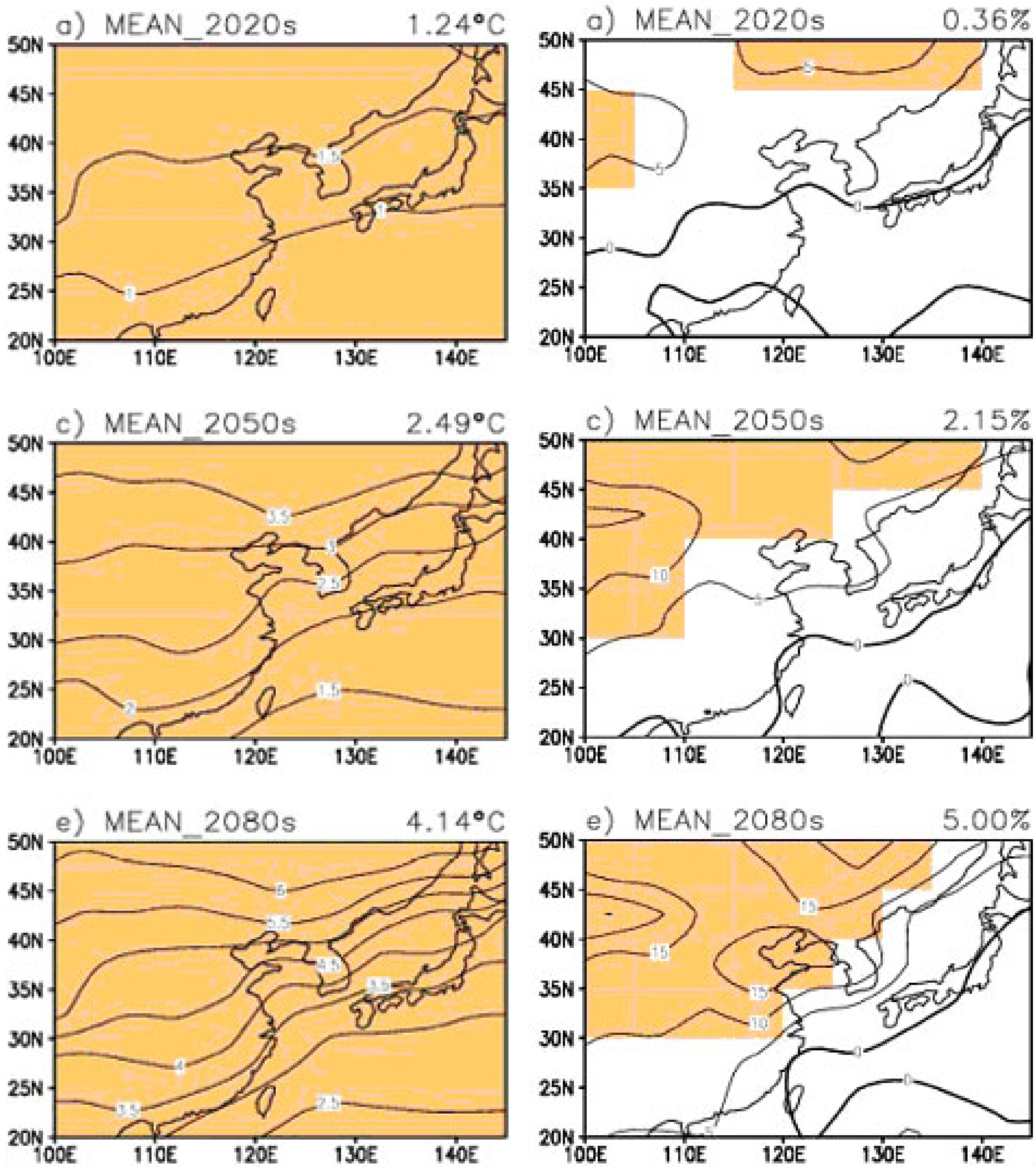

Figure 11.3.4.6. Multi-model ensemble mean of near surface temperature (left) and precipitation change (right) in MME7 for the SRES A2 scenario for the 2020s, 2050s and 2080s. Changes are relative to 1961–1990 mean and the area where ensemble mean is greater than standard deviation is shaded. (Min et al., 2004)

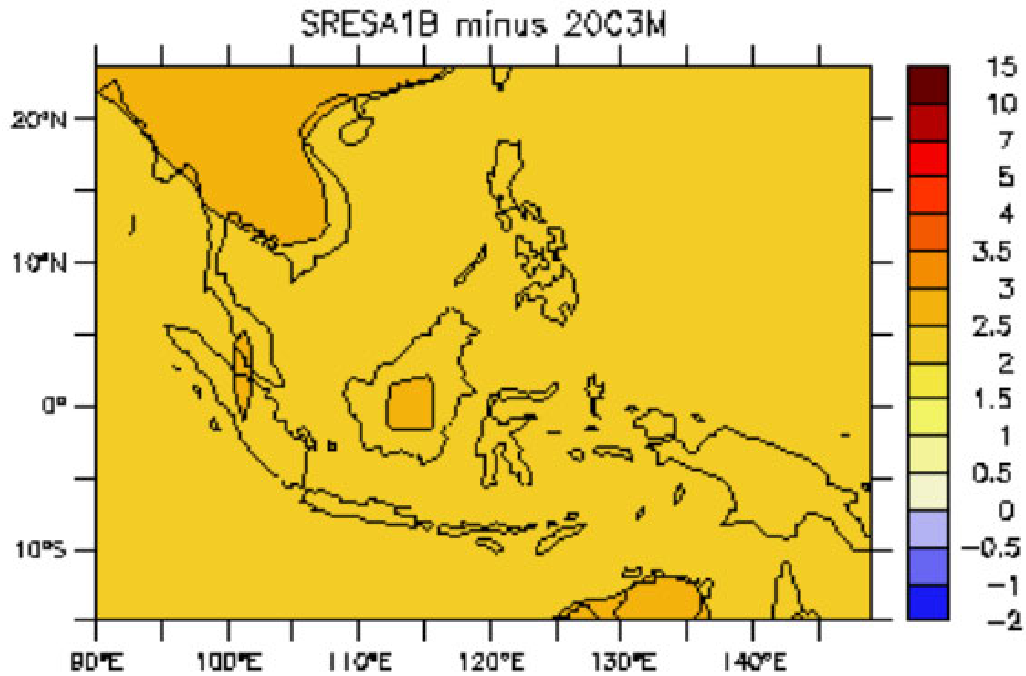

Figure 11.3.4.7. Annual mean warming (surface air temperature1979–1998 to 2079–2098) in A1B averaged over all AR4 simulations.

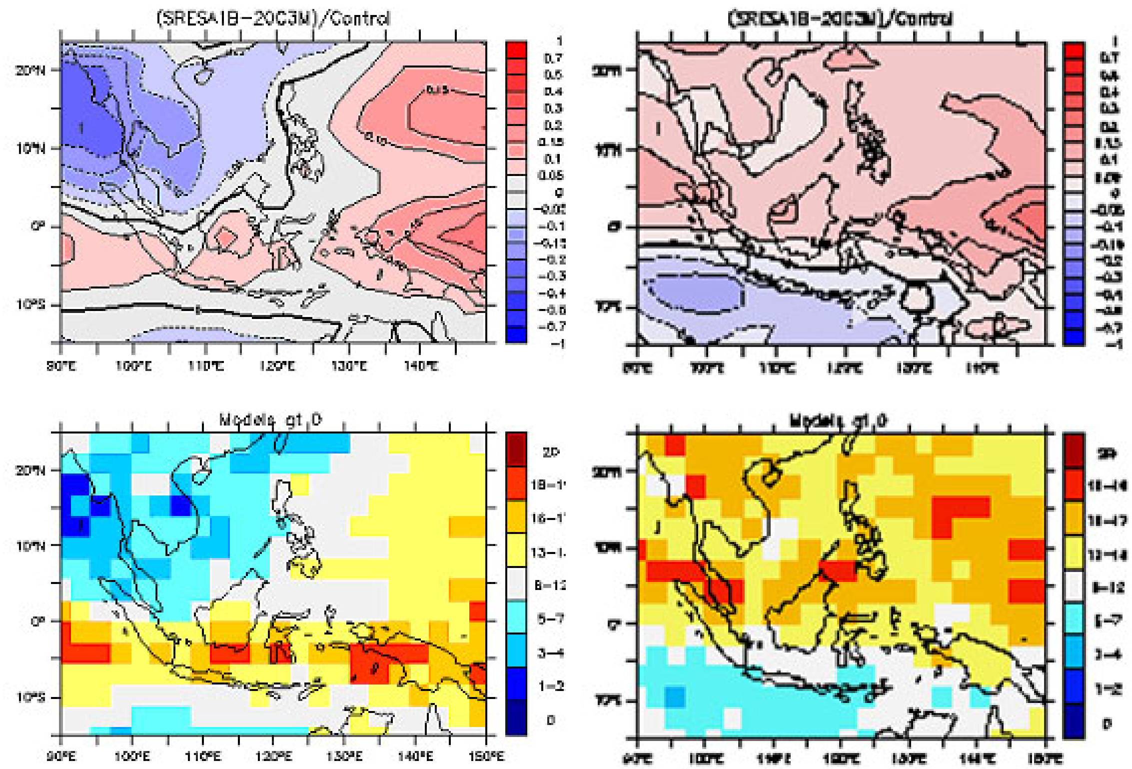

Figure 11.3.4.8. Upper panels: fractional change in precipitation (left-to-right: DJF, JJA) 1979–1998 to 2079–2098 in A1B averaged over all AR4 simulations. Lower panels, number of models projecting increase in precipitation.

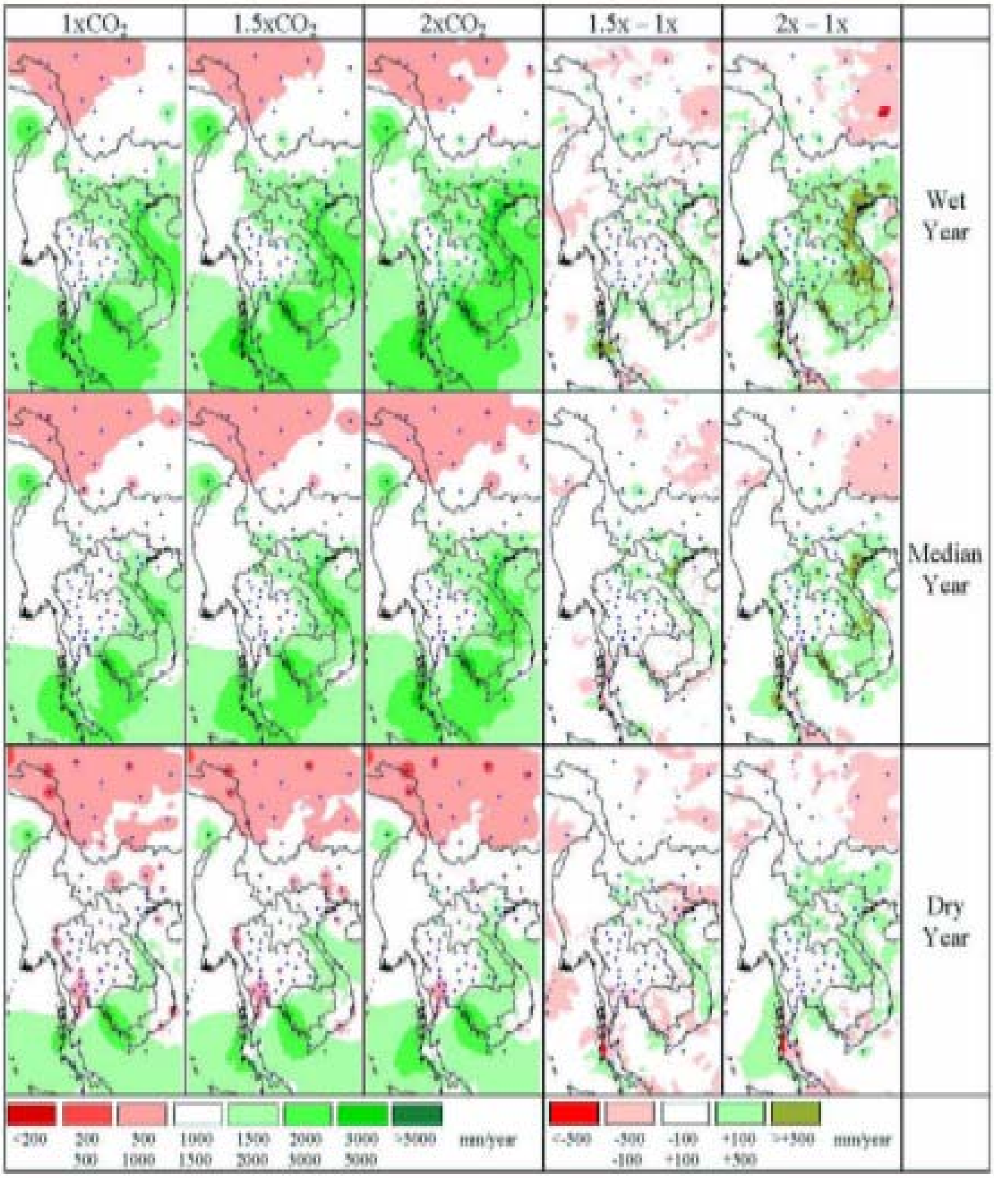

Figure 11.3.4.9. Enhanced greenhouse simulation of precipitation over Indochina using the CSIRO stretched grid model CCAM at 14 km resolution nested in CSIRO Mk 3 (AIAAC, 2004).

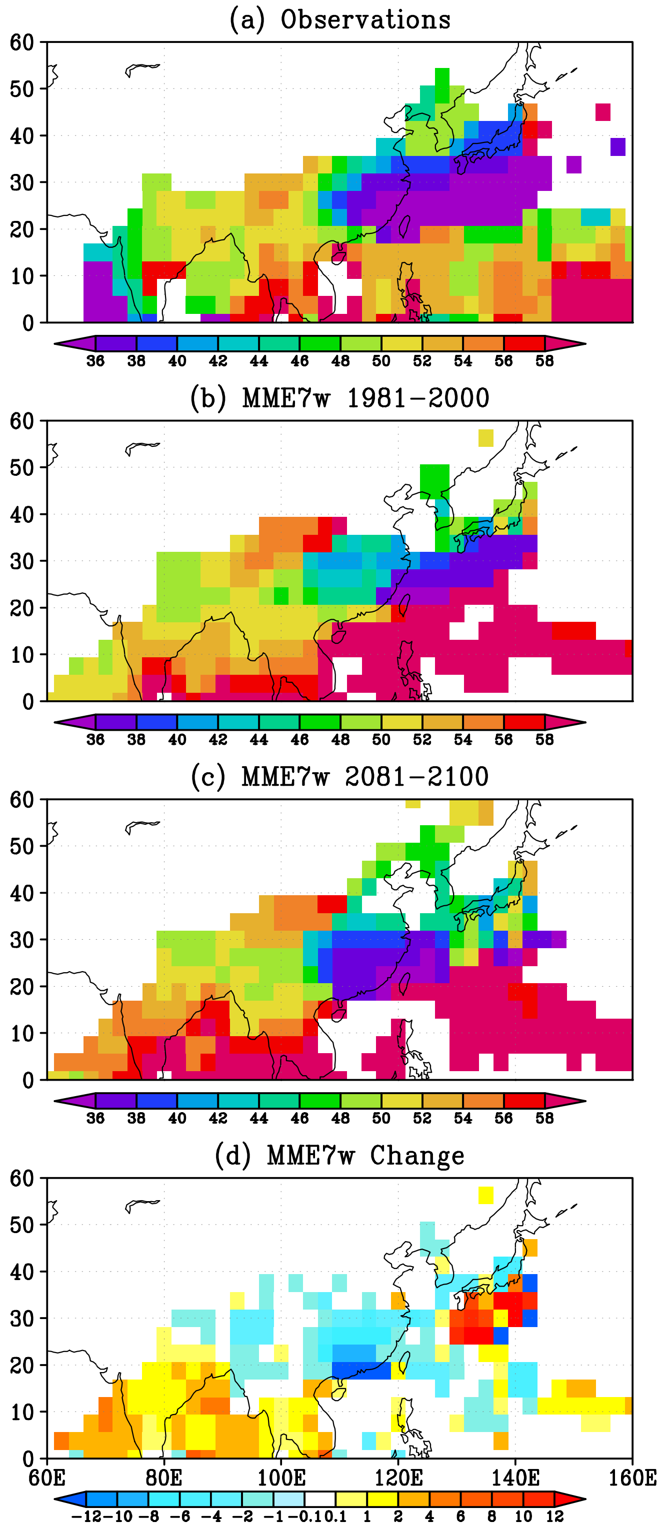

Figure 11.3.4.10. Withdrawal dates (Julian pentad) of the Asian summer rainy season based on the climatological pentad mean precipitation. (a) Observations. (b) Multi-model ensembles for the present day (1981–2000) of the 20C3M experiments. (c) As in (b) except for the 2081–2100 of the SRES A1B experiments. (d) Differences between (c) and (b). (Kitoh and Uchiyama, 2005 Submitted to JMSJ)

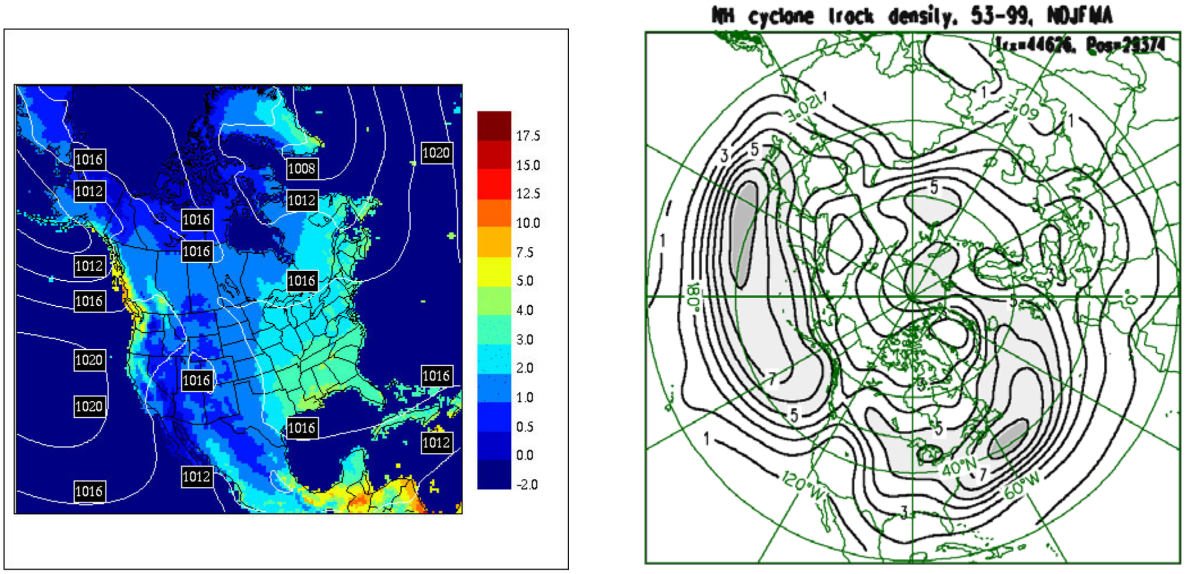

Figure 11.3.5.1. Key regional processes of North America

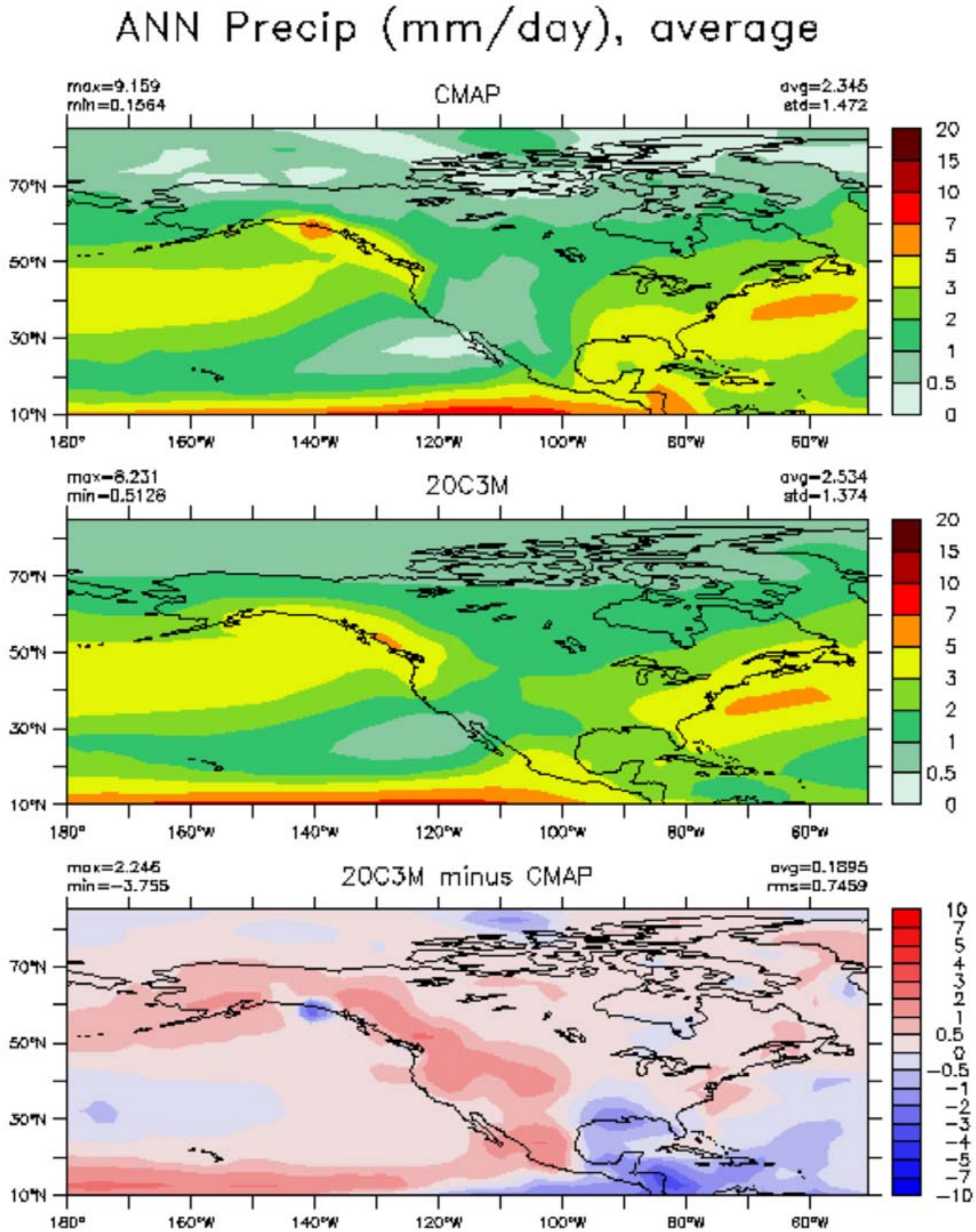

Figure 11.3.5.2. Ensemble-mean simulated annual-mean precipitation from AR4 CGCMs (mm/day)

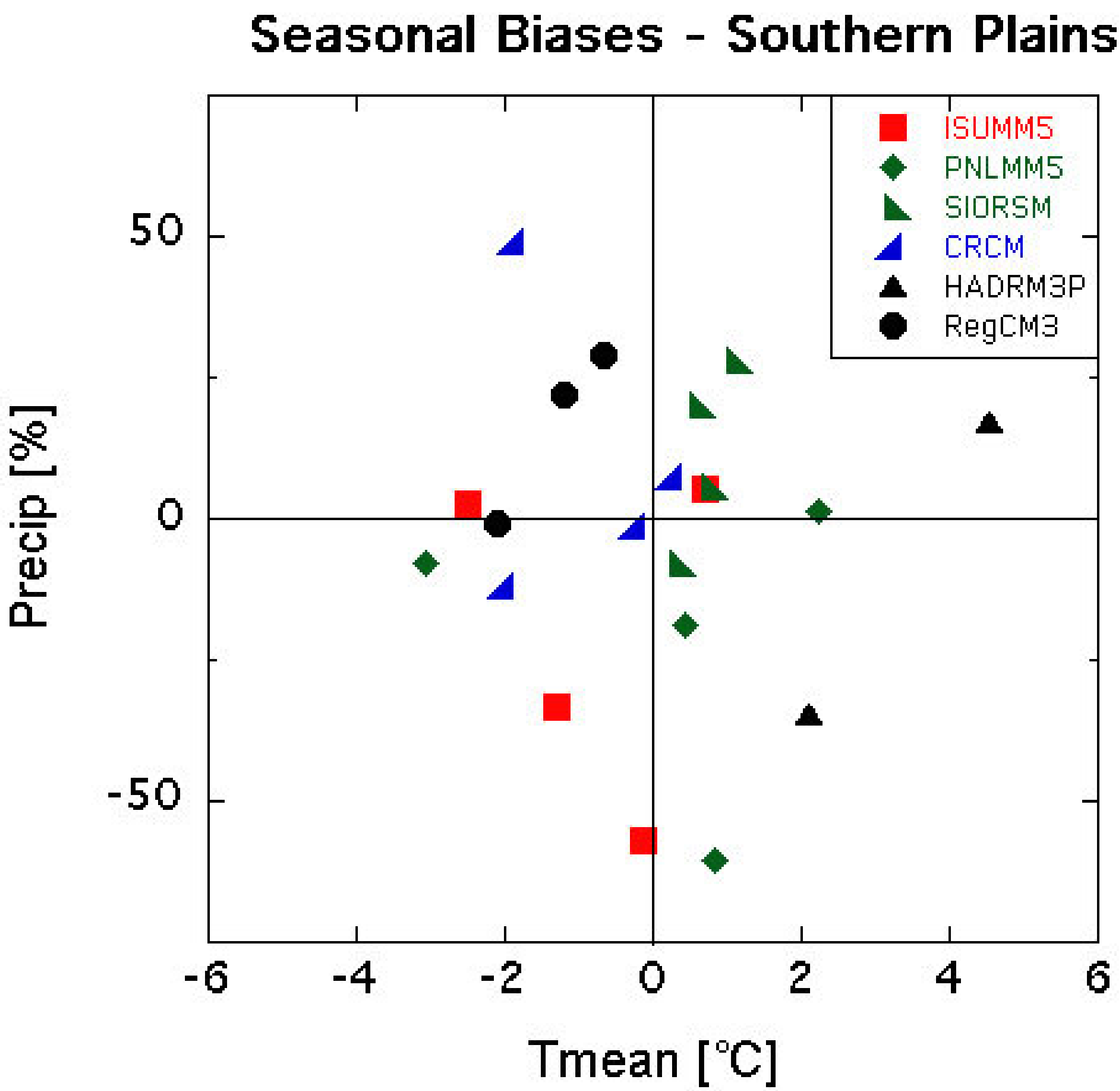

Figure 11.3.5.3. Range of errors for surface air temperature and precipitation for some RCMs participating in NARCCAP.

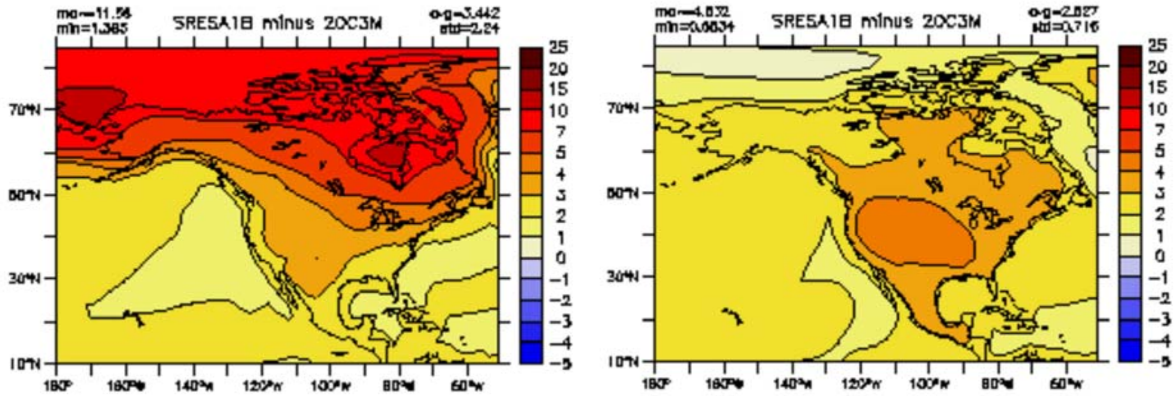

Figure 11.3.5.4. Ensemble-mean projected DJF and JJA surface temperature changes from AR4 CGCMs (°C)